**DE GRUYTER** OPEN

# Annealing and Ni content effects on EPR and structural properties of $Zn_{1-x}Ni_xO$ aerogel nanoparticles

A. Sayari[1,2,*], L. El Mir[3,4]

[1]Department of Physics, Faculty of Science, University of Jeddah, P.O. Box 80327, Jeddah 21589, Saudi Arabia

[2]Université de Tunis El Manar, Faculté des Sciences de Tunis, Unité de recherche Spectroscopie Raman UR13ES31, 2092, Tunis, Tunisia

[3]Al Imam Mohammad Ibn Saud Islamic University (IMSIU), College of Sciences, Department of Physics, Riyadh 11623, Saudi Arabia

[4]Laboratoire de Physique des Matériaux et des Nanomatériaux appliquée à l'Environnement, Faculté des Sciences de Gabès, Cité Erriadh Manara Zrig, 6072 Gabès, Tunisia

$Zn_{1-x}Ni_xO$ aerogel nanopowders with nickel concentration in the range of $0.05 \leqslant x \leqslant 0.25$, were synthesized by the sol-gel processing technique and post-annealed in air at 500 °C. Structural, vibrational, thermal and magnetic properties of the as-prepared and annealed $Zn_{1-x}Ni_xO$ powdered samples were characterized using X-ray diffraction (XRD), transmission electron microscopy (TEM), Raman scattering, thermal gravimetric analysis (TGA) and electron paramagnetic resonance (EPR) spectroscopy. In addition to the ZnNiO phase, XRD analysis revealed the formation of a secondary NiO phase when the Ni content was greater than or equal to 10 %. The TEM images confirm that the particle size is in the range of 20 nm to 40 nm, in accordance with XRD results, and the particles are well dispersed. Raman scattering measurements confirm the wurtzite structure of the synthesized $Zn_{1-x}Ni_xO$ nanopowders and show that intrinsic host-lattice defects are activated when $Ni^{2+}$ ions are substituted to the Zn sites. Room temperature ferromagnetic order was observed in all of the samples and was strongly dependent on the Ni content and thermal annealing. These results indicate that the observed room temperature ferromagnetism in ZnNiO may be attributed to the substitutional incorporation of Ni at Zn sites.

Keywords: *Ni-doped ZnO; nanoparticles; TEM; XRD; Raman scattering; EPR spectroscopy.*

## 1. Introduction

Ferromagnetism (FM) in dilute magnetic oxides infused inside a matrix of a wide band gap semiconductor is one of the most interesting new problems in magnetism due to the emerging spintronic field [1]. As potential candidate, the diluted magnetic semiconductor (DMS) ZnO doped with 3d-transition metals (TMs) or rare-earth elements has attracted a great deal of interest for its magnetic properties since the early theoretical predictions of room temperature ferromagnetic phases in this material [2–7]. TM doped ZnO is one of the most promising DMS candidates as it is predicted to be ferromagnetic above room temperature. Early studies showed ferromagnetism at very low temperatures [8, 9] or no ferromagnetism at all, above 4 K for any 3d TM dopant [10]. The direct super-exchange interaction between TM ions is expected to be antiferromagnetic, as has been experimentally confirmed for Co and Mn doping, while carrier mediated exchange has been proposed to be responsible for the predicted FM behavior [11–13]. In the case of Ni-doped ZnO samples, the origin of ferromagnetism is very complex [14, 15].

Nickel is an important dopant in ZnO semiconductor due to the possibility of replacing $Zn^{2+}$ ions in the ZnO lattice. $Ni^{2+}$ (0.69 Å) ion has the same valence as $Zn^{2+}$ and its radius is close to that of $Zn^{2+}$ (0.74 Å) [16]. Some investigations on Ni doped ZnO have been reported and several results showed that the magnetic and optical properties of ZnO have changed after doping by Ni [17–19]. The results were sensitive to a sample type and the

*E-mail: amor.sayari@laposte.net

preparation method. It has been shown that manipulation of surface states of nanosized ZnO particles gives an additional parameter to influence the magnetic properties of these materials [4]. A variety of chemical methods have been developed to prepare ZnO nanoparticles. Most of the ZnO crystals have been synthesized by traditional high-temperature solid-state method in which it is difficult to control the particle properties. However, ZnO nanoparticles can be prepared at low cost on a large scale by simple solution-based methods such as chemical precipitation, sol-gel process, and hydrothermal reaction [20–24].

We report here the results obtained for Ni doped ZnO aerogel nanopowders prepared by a modified sol gel process. The effects of annealing at 500 °C in air and the Ni dopant concentration on the structural, vibrational and magnetic properties are discussed. We used the electron paramagnetic resonance (EPR) spectroscopy to study incorporation of Ni ions into the ZnO crystalline lattice due to its extreme sensitivity to the microscopic environment of the paramagnetic center. Our results show a strong modification of the $Zn_{1-x}Ni_xO$ nanopowders magnetic properties by annealing and Ni content.

## 2.    Experimental

$Zn_{1-x}Ni_xO$ aerogel nanopowders with dopant concentrations of x = 0.05, 0.10, 0.15, 0.20 and 0.25 were synthesized by dissolving 2 g of zinc acetate dihydrate ($Zn(CH_3COO)_2 \cdot 2H_2O$) in 14 mL of methanol. After 30 min magnetic stirring at room temperature, adequate quantity of nickel chloride hexahydrate ($NiCl_2 \cdot 6H_2O$) was added. After 15 min of magnetic stirring, the solution was placed in an autoclave and dried under supercritical conditions in ethyl alcohol (EtOH) at T = 300 °C. The obtained powders were divided into two parts. The first one was analyzed as-synthesized and the second one was annealed at 500 °C in air for 2 h.

The X-ray diffraction (XRD) patterns of $Zn_{1-x}Ni_xO$ powders were measured with a Bruker D5005 diffractometer, using $CuK\alpha$ radiation ($\lambda = 1.5418$ Å). The transmission electron microscopy (TEM) measurements were performed with a JEM-200CX microscope. For TEM analysis, the synthesized $Zn_{1-x}Ni_xO$ nanopowders were put in EtOH and immersed in an ultrasonic bath for 15 min; a few drops of the resulting suspension were then deposited on the TEM grid. The EPR measurements were performed with a standard X-band (9.5 GHz) spectrometer with 100 KHz modulation and first derivative detection at temperatures between 4 K and 300 K. Thermal gravimetric analysis (TGA) was performed using a TGA apparatus (PerkinElmer). Approximately 2.9 mg of a sample was placed in a platinum crucible on the pan of a microbalance and heated from 35 °C to 950 °C at a rate of 10 °C·min$^{-1}$. The Raman scattering was performed at room temperature with a Labram system equipped with a microscope in back-scattering configuration. The excitation line was 514.5 nm from an Ar$^+$ laser.

## 3.    Results and discussion

### 3.1.    Morphological and structural characterization

Fig. 1 shows the XRD spectra of the as-prepared and annealed $Zn_{0.75}Ni_{0.25}O$ nanopowder samples [25, 26]. The two spectra are dominated by the diffraction peaks of wurtzite ZnO, with preferred orientation along [1 0 1], [1 0 0] and [0 0 2] directions, but also show secondary phase inclusions [27, 28]. Extra peaks that appear at 11° and 16° in the as-prepared sample completely disappear after annealing the sample at 500 °C in air. However, the two peaks with a very weak intensity observed at 37° and 42° in the as-prepared sample, become more intense after annealing. The extra peaks, located at 11°, 16°, 37° and 42° are due to the presence of additional phases in wurtzite ZnO, mainly related to metallic Ni and NiO crystalline structures. It is known that Ni is very unstable in the ZnO matrix and has the tendency to form clusters of metallic Ni or NiO [29]. After annealing of the Ni doped ZnO powders in air at 500 °C, the wurtzite structure of ZnO is unchanged, except the slight shifts of the reflection positions.
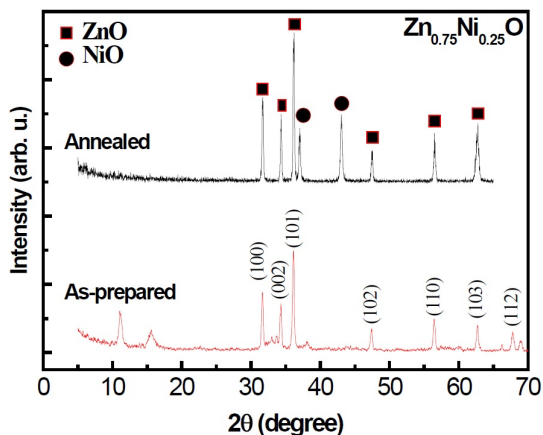
Fig. 1. Comparison of X-ray diffraction spectra of as-synthesized and annealed $Zn_{0.75}Ni_{0.25}O$ nanopowders; observation of NiO phase.

In order to study the effect of Ni content on the secondary phase formation, the XRD patterns of the $Zn_{1-x}Ni_xO$ nanopowders ($0.05 \leqslant x \leqslant 0.25$) annealed in air at 500 °C are presented in Fig. 2. With Ni incorporation, the dominant peaks of ZnO are retained but the extra peaks (at ~37° and 42°) grow in intensity for $x \geqslant 0.1$. Occurrence of the extra peaks and dependence of their intensities on Ni concentration indicate that phase segregation has occurred and the lower solubility limit of Ni in $Zn_{1-x}Ni_xO$ nanoparticles is ~0.1. As the Ni content increases beyond the limit of the solid solubility of Ni in ZnO, part of Ni ions does not enter in the crystalline structure of ZnO and thus crystallizes alone forming nano NiO grains as indicated by the XRD patterns. Such a structural degradation in the ZnO lattice may be attributed to the introduction of a foreign impurity with subsequent annealing [30]. As seen in Fig. 1 and Fig. 2 the diffraction lines are rather broad with the broadening depending on the Miller indices of the corresponding sets of crystal planes. This indicates asymmetry in the crystallite shape. After correction for the instrumental broadening, an average value of the basal diameter of the prism-shaped crystallites was found to be 14 nm to 20 nm, whereas the height of the crystallites was in the range of 25 nm to 39 nm (Table 1) [31]. From Table 1, the crystallite size of the samples increases with increasing Ni

content. Such variation in particle size is evident from Fig. 2. Pure ZnO exhibits broad diffraction peaks when compared to those of nickel doped ZnO samples. TEM measurements show that the as-prepared aerogel powders are composed of nano-sized particles as confirmed by TEM micrograph of the synthesized $Zn_{0.75}Ni_{0.25}O$ sample (Fig. 3). The grain size estimated using TEM micrographs and the 100 nm scale bar ranges from 20 nm to 40 nm. The later values are very similar to those deduced from XRD measurements and the Scherrer equation (Table 1). The strain was also calculated for the $Zn_{1-x}Ni_xO$ powders (Table 1) and was nearly constant for the different Ni contents. From XRD and TEM measurements we can conclude that the annealed $Zn_{1-x}Ni_xO$ particles are single crystalline and no aggregates of smaller crystals are formed.
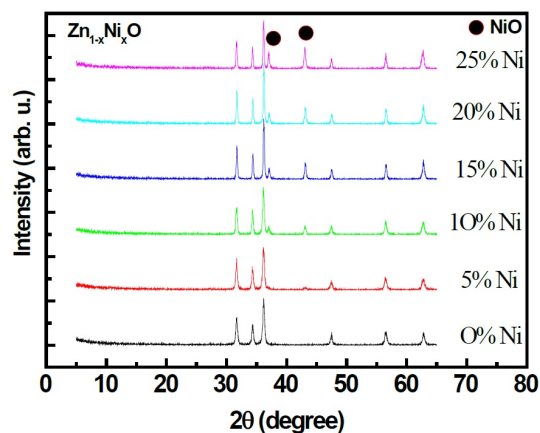


Fig. 2. X-ray diffraction spectra of $Zn_{1-x}Ni_xO$ nanopowders annealed at 500 °C in air for two hours; Ni content dependence of the NiO lines.

Fig. 4 shows the changes of lattice parameters (a and c) of the annealed $Zn_{1-x}Ni_xO$ nanopowders with the Ni content. The lattice constants increase with an increase in the $Ni^{2+}$ concentration until $x = 0.1$ and then decrease. The lattice parameters and the unit cell volume of the $Zn_{1-x}Ni_xO$ nanoparticles (Table 1) are found to be greater than those of undoped ZnO and bulk ZnO (47.58 Å³) [32]. If all the Ni ions were replacing $Zn^{2+}$ ions, no expansion should be expected since Ni ion has a smaller
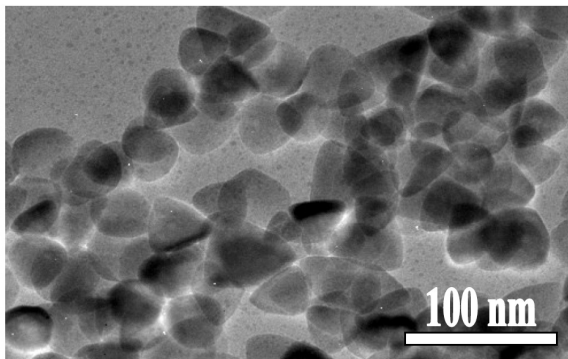
Fig. 3. TEM micrograph of as-synthesized $Zn_{0.75}Ni_{0.25}O$ nanoparticles.

Table 1. Volume of unit cell, strain and crystallite sizes estimated from XRD data of the annealed $Zn_{1-x}Ni_xO$ nanopowders.

| Nickel content [at.%] | Average crystallite size d [nm] | Volume of unit cell [$Å^3$] | Strain $\times 10^{-3}$ |
|---|---|---|---|
| 0 | 25 | 47.919 | 4.7 |
| 5 | 26.8 | 48.012 | 4.5 |
| 10 | 30 | 48.183 | 4 |
| 15 | 36 | 48.061 | 3 |
| 20 | 38 | 48.012 | 3.1 |
| 25 | 39 | 48.038 | 3 |

ionic radius than $Zn^{2+}$ [16]. However, the slight expansion of the lattice indicates that Ni ions are partially located interstitially. Such a result was observed by Strachowski et al. [33] for ZnAlO nanoparticles where Al ions are smaller than the Zn ions. The nonlinearity behavior in our case can be related to the lower solubility of Ni in ZnO and the formation of the secondary phase at high nickel concentration.
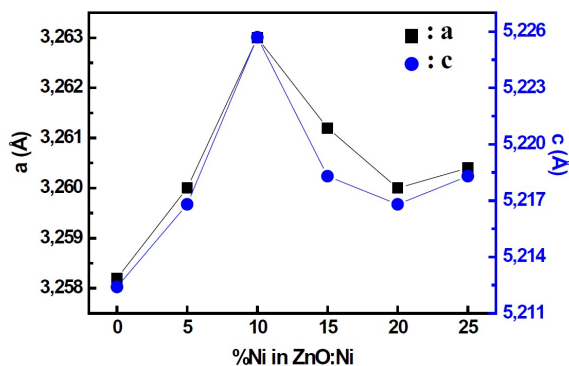


Fig. 4. Ni content dependence of lattice parameters (a, c) of annealed $Zn_{1-x}Ni_xO$ aerogel powders.

## 3.2. Thermal properties

The thermal behavior of the dried $Zn_{1-x}Ni_xO$ gel has been investigated by thermal gravimetric analysis (TGA). Fig. 5 depicts the results of the $Zn_{1-x}Ni_xO$ TGA measurements for x = 0.1 as an example. It can be seen that the sample weight decreases continuously with an increase in temperature (Fig. 5). The decreasing rate for T < 450 °C

is higher than that in the range of T > 450 °C. The TGA curve shows four main regions. The first weight loss, from room temperature up to 150 °C, is due to the dehydration of $Zn_{0.9}Ni_{0.1}O$ nanopowders. The second weight loss, from 150 °C to 220 °C, is attributed to the decomposition of chemically bound groups. The third step from 220 °C to 350 °C is related to the decomposition of the organic groups. The weight loss from 350 °C to 450 °C is attributed to the incorporation of Ni ions in the ZnO lattice and formation mainly of the $Zn_{0.9}Ni_{0.1}O$ phase. Also, the formation of the NiO phase can take place in this step.
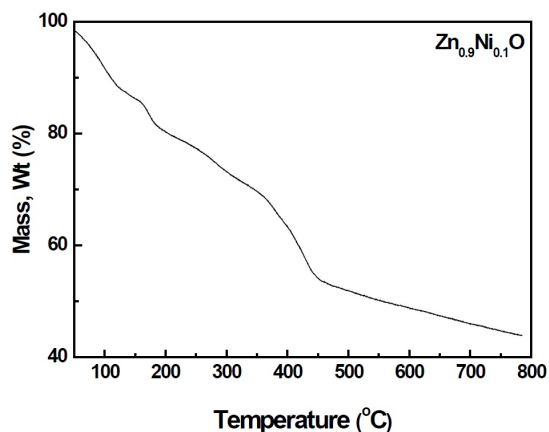


Fig. 5. TGA curve of a $Zn_{0.9}Ni_{0.1}O$ nanopowdered sample.

## 3.3. Raman scattering

The room temperature Raman spectrum of the $Zn_{0.9}Ni_{0.1}O$ sample is reported in Fig. 6 as an example. At the low frequency region, the peaks
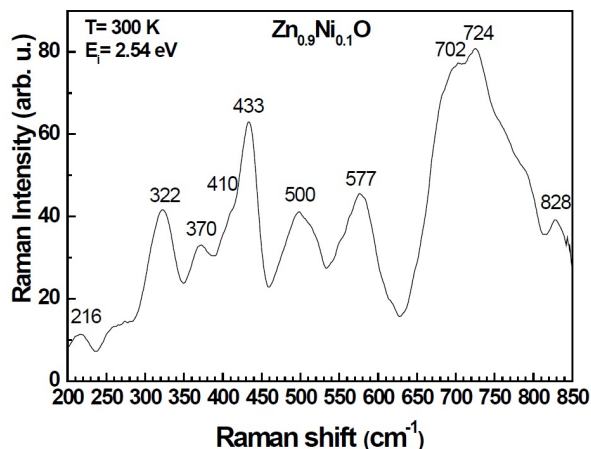
Fig. 6. Room temperature Raman backscattering spectrum of a $Zn_{0.9}Ni_{0.1}O$ nanopowdered sample.

at 216 cm$^{-1}$, 322 cm$^{-1}$, 370 cm$^{-1}$ and 410 cm$^{-1}$ are attributed, respectively, to 2E$_2$(low), 2E$_2$(M), transverse optical (TO) A$_1$ and E$_1$(TO) modes [34]. Phonons in a nanocrystal are confined in space and all types of phonons over the entire Brillouin zone will contribute to the Raman spectrum. The intense peak at $\sim$433 cm$^{-1}$ is the E$_2$(high) mode, characteristic of the ZnO crystallinity [35]. The observation of these modes indicates that the ZnNiO products have a wurtzite structure as confirmed by XRD analysis. The large and relatively intense peak located at about 500 cm$^{-1}$ is a disorder-activated Raman scattering and could be due to doped impurities or crystal defects such as oxygen vacancies and Zn interstitials [36]. The broad Raman peak at around 577 cm$^{-1}$ may be due to the longitudinal optical A$_1$ mode [37]. Recent reports have related the appearance of this mode to lattice defects, being either oxygen vacancies or zinc interstitials or their combination [38, 39]. At the high frequency region, the broad and high intense peak centered at $\sim$713 cm$^{-1}$ and the weak peak at 828 cm$^{-1}$ can be assigned to additional modes which may be associated with Ni$^{2+}$ ions occupation at the Zn sites. Raman results show that lattice defects are introduced and intrinsic host-lattice defects are activated when Ni$^{2+}$ ions are substituted to the Zn sites. The Raman bands centered at 560 cm$^{-1}$ and 740 cm$^{-1}$ can be attributed, respectively, to the LO and two-phonon TO modes of the NiO phase [40].
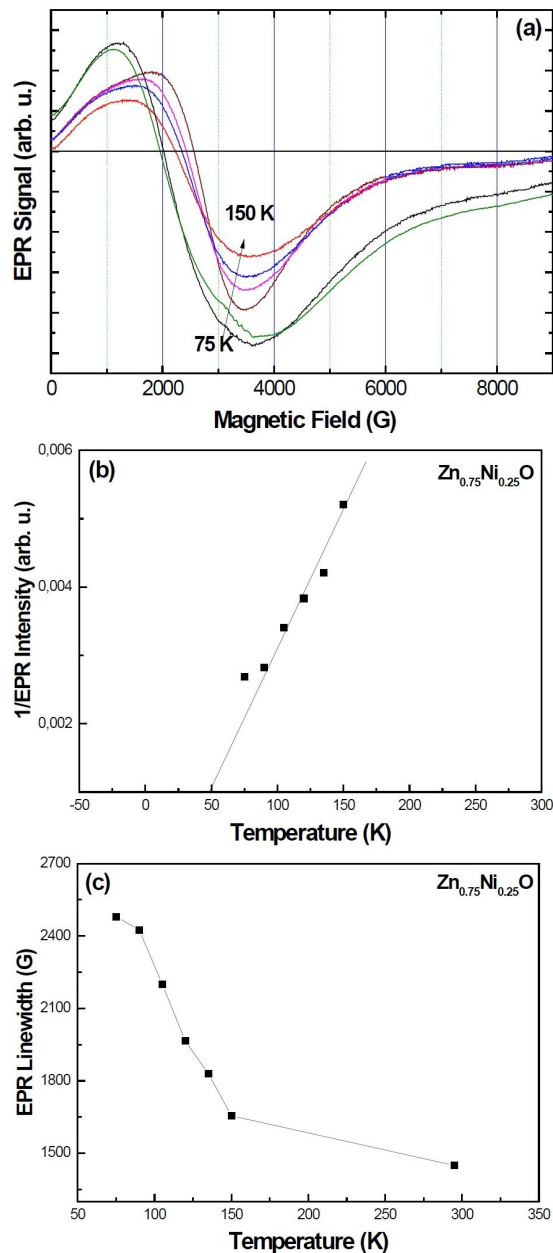


Fig. 7. Temperature dependence of an EPR spectrum of a $Zn_{0.75}Ni_{0.25}O$ nanopowder sample in the temperature range between 75 and 150 K with a step of 15 K (a); temperature dependence of inverse intensity of the EPR signal (b) and $\Delta H$ (c).

## 3.4. Electron paramagnetic resonance (EPR)

The roles of exchange interaction and the defect centers in DMSs are understood from

EPR spectra [41]. The evolution with temperature of the EPR signal, the peak to peak line width $\Delta H$ and the inverse of EPR intensity of the as-synthesized $Zn_{0.75}Ni_{0.25}O$ sample are shown in Fig. 7. The EPR spectra are characterized by a very broad lines extending from 0 G to 8500 G with g-values varying from 2.5 to 2.78, respectively, for temperatures 150 K and 75 K. These lines are characteristic of the presence of FM particles (g > 2) with shape and orientation distribution. The line width and the g-values of the $Zn_{0.75}Ni_{0.25}O$ EPR signal in our work are consistent with the line shapes and positions of the previously reported results on Ni-doped ZnO samples [42] and have been attributed to a ferromagnetic resonance caused by $Ni^{2+}$ ions. It could be observed that the EPR intensity and the line width increase with lowering of the temperature until the blocking value (T = 150 K). However, below this temperature the resonance field shifts to lower fields and the EPR signal becomes broad and intense. The $\Delta H$ values for the temperatures 75 K and 150 K are 2560 G and 1622 G, respectively (Fig. 7c). Such temperature dependent changes in the field position and line width of the EPR signal occur in the ferromagnetic state because these depend on the magnetization and the anisotropy constant, which are temperature dependent in a ferromagnet [43]. Direct information about the magnetic state can be obtained from the variation of intensity of the EPR signal with temperature [43]. EPR intensity is directly proportional to the spin susceptibility $\chi$ of the paramagnetic species taking part in resonance. Fig. 7b displays the temperature dependence of the quantity $\chi^{-1}$. The linear increase of $\chi^{-1}(T)$ at higher temperatures can be fitted to the Curie-Weiss law. The line is a linear extrapolation illustrating the paramagnetic Curie-Weiss temperature ($\theta_{cw} = 50$ K). The positive sign of the Curie-Weiss temperature indicates that some of the Ni ions are ferromagnetically coupled in this sample.

Fig. 8 shows the room temperature EPR spectra, observed in the $Zn_{1-x}Ni_xO$ samples after annealing at 500 °C in air for 2 h. The EPR spectra are strongly modified by the annealing treatment for all the Ni contents. A comparison between the EPR spectra of the samples annealed and as-synthesized with x = 0.25 is shown in the inset of Fig. 8. It is clear that the EPR signal for the non-annealed sample is broader and has a larger value of g compared to the annealed one. The EPR line widths for the as-synthesized and annealed samples are 1471 G and 583 G, respectively. This may be understood by the combined effects of air-annealing induced increase in free carrier concentration and the lattice relaxation. The different values of g and the EPR line width for the annealed samples with different Ni contents are given in Table 2. All EPR spectra exhibit symmetric and narrow resonance signals centered around 3150 G field. From Fig. 8, it is clear that the amplitude of the EPR signal increases while the value of the resonant field slightly decreases with increasing the Ni concentration. When the nickel content increases, the average distance between $Ni^{2+}$ and $Ni^{2+}$ ions decreases and the super-exchange interactions between these neighboring $Ni^{2+}$ ions increase the internal field [44] and decrease the resonant field. Similar results on Ni-doped ZnO nanoparticles were reported, which also revealed a broad signal due to long range exchange interactions of $Ni^{2+}$ ions with g-values in the range of 2.2 to 2.57 [15, 42]. The EPR signal for the $Zn_{0.75}Ni_{0.25}O$ sample exhibits an intense resonance with a g-value of 2.199 and a line width of 583 G at 295 K. The g-factor, linewidth and line-shape are characteristic of the presence of superparamagnetic Ni nanoparticles [45]. The interactions may be a combination of exchange and dipolar nature. The magnetic moments from the surface of grains offer dipolar effects for the low values of Ni contents. However, when the Ni content has increased to x = 0.25 in ZnO:Ni nanoparticles the surface of the grains may tend to accommodate more nickel, hence, there is an appreciable exchange effect in this case [46]. For high Ni concentrations, a narrower peak appears at higher magnetic fields with g-value much less dependent on the doping concentration. The narrow EPR signal having a g-value of 1.96 can be assigned to oxygen vacancies formed in the ZnO crystallites [47–49]. In general, this signal is common for bulk ZnO ceramics and powders and will be observed in nanocrystals with diameters larger than 20 nm, due to the random orientations of the nanocrystals [50].
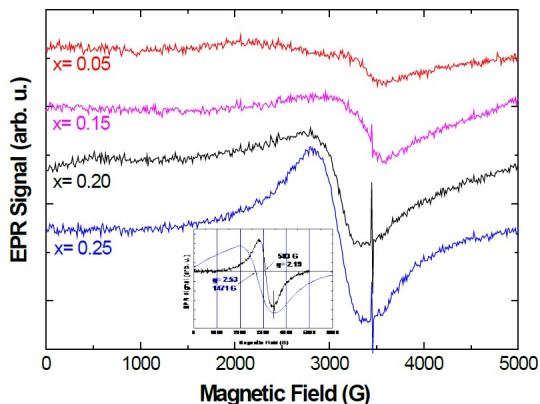
Fig. 8. Ni content dependence of room temperature EPR spectra of annealed $Zn_{1-x}Ni_xO$ aerogel powders. Inset: comparison of room temperature EPR spectra of as-synthesized and annealed $Zn_{0.75}Ni_{0.25}O$ nanoparticles.

Table 2. Resonance field, g-factor and peak to peak line width of EPR signal of the annealed $Zn_{1-x}Ni_xO$ nanoparticles.

| Nickel content [at.%] | Resonance field [G] | g-Factor | $\Delta H_{pp}$ [G] |
|---|---|---|---|
| 5 | 3222.12 | 2.106 | 1471 |
| 15 | 3211.47 | 2.113 | 755 |
| 20 | 3102.05 | 2.188 | 638 |
| 25 | 3086.18 | 2.199 | 583 |

To study the temperature effect on the magnetic properties of the annealed $Zn_{1-x}Ni_xO$ samples, the EPR spectra obtained at different temperatures for x = 0.25, shown in Fig. 9, have been analyzed. It is clear that the EPR signal is composed of two lines for the temperatures 160 K < T ⩽ 295 K: the broad line A at g ∼ 2.27 and the fine line B at g ∼ 2.05. The broad EPR signal has very unusual temperature dependence. The line position of signal A does not shift with temperature (∼2987 G) and its line shape stays symmetric. However, the line width of signal A broadens when the temperature is decreased from 295 K and its intensity decreases until T = 160 K. At this temperature another fine line C with a g-value of 1.995 emerges in the EPR spectrum. For T < 160 K, the intensity of signal A increases again and its line width increases until T = 60 K. At low temperatures, signal

A shows a drastic change, its intensity decreases again but its line width increases. The intensity of the two fine lines increases and their line widths broaden. At T = 20 K, signal A disappears from the EPR spectrum and the two fine lines B and C dominate completely the EPR signal. The observed effect is a complete transformation of one spectrum into another at critical temperatures of 30 K and 150 K. The broad signal must be related to a specific compound with well-defined phase transitions probably due to vigorous fluctuation of the perturbation from the crystal lattice induced by thermal effect. However, the sharp lines B and C with independent resonance fields on temperature and observed at g ∼ 2.05 and g ∼ 1.995 can be attributed to shallow donor and singly charged oxygen vacancy, respectively [51]. Further investigations are necessary to clarify why two transition temperatures are operative in this case as for a given superparamagnetic system only one is expected.
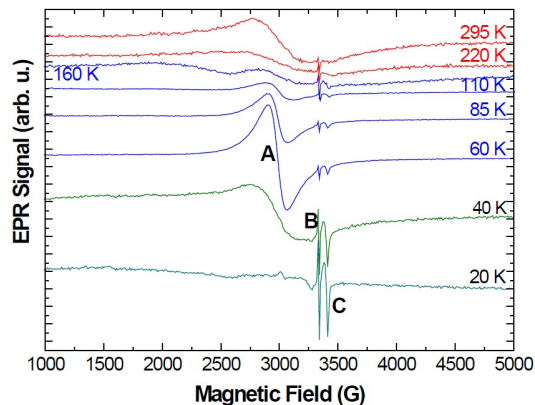


Fig. 9. Temperature dependence of EPR spectra of an annealed $Zn_{0.75}Ni_{0.25}O$ nanopowder sample.

Finally, the origin of ferromagnetism in ZnO-based DMSs is still in debate and has a number of possibilities. The possibility that ferromagnetism can originate from the NiO secondary phase formed in ZnNiO nanoparticles, could be easily ruled out because NiO exhibits antiferromagnetism with a Neel temperature of 520 K [52], and in the nanocrystalline form, NiO shows weak ferromagnetic behavior. Another possible secondary phase is the presence of a Ni metallic phase. However,

there is no indication of Ni metal in the EPR spectra. Therefore, the existence of Ni metal in the Ni-doped ZnO samples can also be excluded. Thus, we can consider ferromagnetism as intrinsic in origin derived from the substitution of $Ni^{2+}$ ions for $Zn^{2+}$ without changing the wurtzite structure. In the carrier-mediated exchange mechanisms pertinent to magnetism, defects are important to the ferromagnetism of DMSs [53, 54]. Previous studies [55–59] proposed that uncontrolled formation of lattice defects can generate carriers that mediate ferromagnetic ordering. As native point defects, such as O vacancies and Zn interstitials are very common in ZnO, they are likely to contribute to the observed ferromagnetism in the ZnNiO samples rather than any metastable secondary phase. However, the mechanism of the room temperature ferromagnetism for the ZnNiO nanoparticles should be further studied in detail.

## 4.  Conclusions

In summary, Ni doped ZnO nanoparticles, with 25 nm to 39 nm average crystallite size, have been successfully synthesized by a modified sol-gel process. Both annealing and Ni content effects on the structural and magnetic properties are investigated. XRD analysis reveals the formation of hexagonal wurtzite structure for all the annealed $Zn_{1-x}Ni_xO$ nanoparticles and shows the existence of secondary NiO phase in the samples with $x \geqslant 0.1$. Raman scattering measurements confirm the wurtzite crystalline structure of the $Zn_{1-x}Ni_xO$ nanopowders and the existence of intrinsic host-lattice defects which are activated when $Ni^{2+}$ ions are substituted to the Zn sites. EPR analysis demonstrates that magnetic properties of the $Zn_{1-x}Ni_xO$ nanopowders are strongly dependent on Ni content and thermal annealing. Our results indicate that the observed room temperature ferromagnetism for Zn-NiO could originate from the long-range $Ni^{2+}$ to $Ni^{2+}$ ferromagnetic coupling mediated by shallow donor electrons rather than due to any impurity phase. Further investigations are necessary to understand the room temperature mechanism and to clarify why two transition temperatures are operative in our case.

## References

[1] WOLF S.A., AWSCHALOM D.D., BUHRMAN R.A., DAUGHTON J.M., MOLNAR VON S., ROUKES M.L., CHTCHELKANOVA A.Y., TREGER D.M., *Science*, 294 (2001), 1488.

[2] RODE K., ANANE A., MATTANA R., CONTOUR J.-P., DURAND O., LE BOURGEOIS R., *J. Appl. Phys.*, 93 (2003), 7676.

[3] PRELLIER W., FOUCHET A., MERCEY B., SIMON C., RAVEAU B., *Appl. Phys. Lett.*, 82 (2003), 3490.

[4] RADOVANOVIC P.V., GAMELIN D.R., *Phys. Rev. Lett.*, 91 (2003), 157202.

[5] KITTILSTVED K.R., GAMELIN D.R., *J. Am. Chem. Soc.*, 127 (2005), 5292.

[6] SONG C., PAN S.N., LIU X.J., LI X. W., ZENG F., YAN W. S., HE B., PAN F., *J. Phys.-Condens. Mat.*, 19 (2007), 176229.

[7] PAN F., SONG C., LIU X., YANG Y., ZENG F., *Mat. Sci. Eng. R*, 62 (2008), 1.

[8] ANDO K., SAITO H., JIN Z., FUKUMURA T., KAWASAKI M., MATSUMOTO Y., KOINUMA H., *Appl. Phys. Lett.*, 78 (2001), 2700.

[9] NORTON D.P., PEARTON S.J., HEBARD A.F., THEODOROPOULOU N., BOATNER L.A., WILSON R. G., *Appl. Phys. Lett.*, 82 (2003), 239.

[10] JIN Z., FUKUMURA T., KAWASAKI M., ANDO K., SAITO H., SEKIGUCHI T., YOO Y.Z., MURAKAMI M., MATSUMOTO Y., HASEGAWA T., KOINUMA H., *Appl. Phys. Lett.*, 78 (2001), 3824.

[11] JANISCH R., GOPAL P., SPALDIN N.A., *J. Phys.-Condens. Mat.*, 17 (2005), R657.

[12] SESHADRI R., *Curr. Opin. Solid State Mater. Sci.*, 9 (2005), 1.

[13] LIU C., YUN F., MORKOC H., *J. Mater. Sci.-Mater. El.*, 16 (2005), 555.

[14] AZZONI C.B., PALEARI A., MASSAROTTI V., CAPSONI D., *J. Phys.-Condens. Mat.*, 8 (1996), 7339.

[15] SALAH R., DJAJA N.F., PRAKOSO S. P., *J. Alloy. Compd.*, 546 (2013), 48.

[16] ROBERTS B.K., PAKHOMOV A.B., SHUTTHANANDAN V.S., KRISHNAN K.M., *J. Appl. Phys.*, 97 (2005), D310.

[17] CHENG C.W., XU G.Y., ZHANG H.Q., LUO Y., *Mater. Lett.*, 62 (2008), 1617.

[18] SAYARI A., MIR EL L., BARDELEBEN VON H.J., *Eur. Phys.-J. Appl. Phys.*, 67 (2014), 10401.

[19] WU D.W., YANG M., HUANG Z.B., YIN G.F., LIAO X.M., KANG Y.Q., CHEN X.F., WANG H., *J. Colloid Interf. Sci.*, 330 (2009), 380.

[20] SCHWARTZ D.A., KITTILSTVED K.R., GAMELIN D.R., *Appl. Phys. Lett.*, 85 (2004), 1395.

[21] MIR EL L., GHRIBI F., HAJIRI M., AYADI BEN Z., DJESSAS K., CUBUKCU M., BARDELEBEN VON H.J., *Thin Solid Films*, 519 (2011), 5787.

[22] MIR EL L., AYADI BEN Z., RAHMOUNI H., GHOUL EL J., DJESSAS K., BARDELEBEN VON H.J., *Thin Solid Films*, 517 (2009), 6007.

[23] Zhang H., Yang D., Ma X., Ji Y., Xu J., Que D., *Nanotechnology*, 15 (2004), 622.

[24] Sayari A., Mir El L., *Kona Powder Part. J.*, 32 (2015), 154.

[25] Mir El L., Bardeleben von H.J., Saadoun M., Mahmoud Ben A., Cantin J.-L., *Mater. Res. Soc. Symp. Proc.*, 957 (2007), K10-17.

[26] Mir El L., Mahmoud Ben A., Bardeleben von H.J., Cantin J.-L., *Mater. Res. Soc. Symp. Proc.*, 957 (2007) K10-16.

[27] Li W.J., Shi E.W., Yin Z.W., *J. Mater. Sci. Lett.*, 20 (2001), 1381.

[28] Liu B., Zeng H.C., *J. Am. Chem. Soc.*, 125 (2003), 4430.

[29] Shen G.Z., Cho J.H., Yoo J.K., Yi G.C., Lee C.J., *J. Phys. Chem. B*, 109 (2005), 5491.

[30] Mohapatra J., Mishra D.K., Kamilla S.K., Medicherla V.R.R., Phase D.M., Berma V., Singh S.K., *Phys. Status Solidi B*, 248 (2011), 1352.

[31] Sharma P.K., Dutta R.K., Pandey A.C., *J. Magn. Magn. Mater.*, 321 (2009), 3457.

[32] Cullity B.D., Stock S.R., *Elements of X-ray Diffraction*, Prentice Hall, New York, 2001.

[33] Strachowski T., Grzanka E., Lojkowski W., Presz A., Godlewski M., Yatsunenko S., Matysiak H., Piticescu R.R., Monty C.J., *J. Appl. Phys.*, 102 (2007), 073513.

[34] Swanson H.E., Fuyat R.K., *Natl. Bur. Stand. Circ.*, 2 (1953), 25.

[35] Calleja J.M., Cardona M., *Phys. Rev. B*, 16 (1977), 3753.

[36] Damen T.C., Porto S.P.S., Tell B., *Phys. Rev.*, 142 (1966), 570.

[37] Sayari A., Marzouki A., Lusson A., Oueslati M., Sallet V., *Thin Solid Films*, 518 (2010), 6870.

[38] Cusco R., Alarcon-Llado E., Ibanez J., Artus L., Jimenez J., Wang B., Callahan M.J., *Phys. Rev. B*, 75 (2007), 165202.

[39] Chen Z.Q., Kawasuso A., Xu Y., Naramoto H., Yuan X. L., Sekiguchi T., Suzuki R., Ohdaira T., *Phys. Rev. B*, 71 (2005), 115213.

[40] Ulmane N.M., Kuzmin A., Sildos I., Pärs M., *Cent. Eur. J. Phys.*, 9 (2011), 1096.

[41] Kaschner A., Haboeck U., Strassburg M., Kaczmarczyk G., Hoffmann A., Thomsen C., Zeuner A., Alves H. R., Hofmann D.M., Meyer B.K., *Appl. Phys. Lett.*, 80 (2002), 1909.

[42] Sati P., Pashchenko V., Stepanov A., *Low Temp. Phys.+*, 33 (2007), 1222.

[43] Srinivas K., Manjunath Rao S., Venugopal Reddy P., *J. Nanopart. Res.*, 13 (2011), 817.

[44] Jedrecy N., Bardeleben von H.J., Zheng Y., Cantin J.L., *Phys. Rev. B*, 69 (2004), 041308.

[45] Liu X., Lin F., Sun L., Cheng W., Ma X., Shi W., *Appl. Phys. Lett.*, 88 (2006), 062508.

[46] Sharma V.K., Baiker A., *J. Chem. Phys.*, 75 (1981), 5596.

[47] Krithiga R., Chandrasekaran G., *J. Mater. Sci.-Mater. El.*, 22 (2011), 1229.

[48] Laiho R., Vlasenko L.S., Vlasenko M.P., *J. Appl. Phys.*, 103 (2008), 123709.

[49] Schneider J.J., Hoffmann R.C., Ensgtler J., Klyszcz A., Erdem E., Jakes P., Eichel R.-A., *Chem. Mater.*, 22 (2010), 2203.

[50] Kappers L.A., Gilliam O.R., Evans S.M., Halliburton L.E., Giles N.C., *Nucl. Instrum. Meth. B*, 266 (2008), 2953.

[51] Hofmann D.M., Zhou H., Pfisterer D.R., Alves H., Meyer B.K., Baranov P., Romanov N., Mello de D.C., Meijering A., Orinskii S., Blok H., Schmidt J., *Phys. Status Solidi C*, 1 (2004), 908.

[52] Li D., Leung Y.H., Djurišic A.B., Liu Z.T., Xie M.H., Shi S.L., Xu S.J., Chan W.K., *Appl. Phys. Lett.*, 85 (2004), 1601.

[53] Yilmaz S., MC Glynn E., Bacaksiz E., Cullen J., Chellappan R.K., *Chem. Phys. Lett.*, 525 (2012), 72.

[54] Kittilstved K.R., Norberg N.S., Gamelin D.R., *Phys. Rev. Lett.*, 94 (2005), 147209.

[55] Kittlstved K.R., Liu W.K., Gamelin D.R., *Nat. Mater.*, 5 (2006), 291.

[56] Dietl T., Ohno H., Matsukura F., Cibert J., Ferrand D., *Science*, 287 (2000), 1019.

[57] Dietl T., *Semicond. Sci. Tech.*, 17 (2002), 377.

[58] Sato K., Katayama-Yoshida H., *Semicond. Sci. Tech.*, 17 (2002), 367.

[59] Sato K., Katayama-Yoshida H., *Physica E*, 10 (2001), 251.